

Change of the Electronic Conductivity of Graphene Nanoribbons and Carbon Nanotubes Caused by a Local Deformation

Masato Ohnishi

Department of Nanomechanics, School of Engineering,
Tohoku University, Sendai, Japan
masato.ohnishi@rift.mech.tohoku.ac.jp

Ken Suzuki, and Hideo Miura

Fracture and Reliability Research Institute (FRRI),
School of Engineering, Tohoku University, Sendai, Japan

Abstract—Since the discovery of carbon nanotubes (CNTs), graphene and graphene nanoribbons (GNRs), many efforts have been made to apply these carbon nanomaterials to electronic devices and sensors. Strain sensitivity of CNTs and GNRs is one of their unique electronic properties. However, the effect of complex strain field such as buckling deformation on the electronic state of CNTs remains to be unclear. In this study, we investigated the relationship between the electronic state and the local geometrical structure of deformed CNTs and GNRs. Comparing the electronic state of CNTs and that of GNRs under deformation, we found that the electronic state can be predicted by analyzing the geometric structure of deformed CNTs or GNRs.

Keywords—carbon nanotube, graphene nanoribbon, strain, electronic state

I. INTRODUCTION

Since the discovery of carbon nanotubes (CNTs), both theoretical and experimental studies have revealed their outstanding characteristics [1]-[3]. Both the electronic and mechanical properties of CNTs are better than conventionally used metals and their specific weight is rather light. In addition, they are deformed easily [4], [5] and stable chemically. If the resistivity of CNTs changes drastically comparing with metals, it is, therefore, possible to develop a highly sensitive strain sensor [6], [7].

Thus, we also have proposed a new highly sensitive strain sensor using a popular resin in which CNTs are dispersed uniformly. It is easy to make a cheap, flexible and stable sensor by using the CNT-dispersed resin. The measured change rate was 400%/%-strain under tensile strain and 150%/%-strain under compressive strain, respectively. These values were about a hundred times higher than that of metallic strain gauges. So, the possibility of highly sensitive strain measurement was validated. However, there was large fluctuation of the measured change rate (strain sensitivity) among test samples. Thus, it is very important to clarify the mechanism of the fluctuation of the change rate of the strain sensors using CNTs.

In order to discuss the relationship between the deformation of a CNT and its electronic conductivity, both a

molecular dynamics analysis and the DFT were applied. In this study, various kinds of single-walled carbon nanotube (SWNT) structures were modeled for the analyses. The change of the electronic band structure of SWNTs under uniaxial strain was analyzed by applying the ab initio calculation based on DFT. Since a CNT consists of a six-membered carbon ring, the change of the band structure of a graphene nanoribbon (GNR) was also analyzed by applying the DFT.

II. GEOMETRICAL ANALYSIS OF CNTS

It is well known that the resistance of CNTs changes drastically under uni-axial strain [7]-[12]. Stampfer et al. showed large gauge factors of about 2900 experimentally [12], where a gauge factor is a ratio of change in resistance to amplitude of strain. The conductivity of CNTs is changed by causing their deformation and its change rate varies depending on the geometric configuration of a CNT. This means that it is very important to understand how the geometric configuration of a CNT is changed due to the applied external force for developing the CNT-based two-dimensional strain sensor.

In this section, deformation characteristics of CNTs under a uni-axial strain were analyzed by molecular dynamics (MD). The simulation cell consisted of a (17,0) CNT, and its length was 100.7 Å and the number of carbon atoms was 1632. The CNT was placed in the middle of the cell because the three-dimensional periodic boundary condition was assumed in all the simulations. The basal surface area was large enough ($> 100 \text{ \AA} \times 100 \text{ \AA}$) that the interaction among CNTs in next cells could be neglected. The height of the cell was equal to the length of the CNT. The Tersoff potential of LAMMPS package was used in all the simulations [13]. First, all the simulations were performed under the NPT (300K, 1atm) conditions to acquire the equilibrium state. In each case, the obtained structure was assumed to be under stress (strain)-free condition. Then, the height of the cell was changed at the constant velocity of 2.0 m/s for the loading analysis. In this analysis, x and y coordinates of atom sat both ends were fixed during the change of volume. Analysis conditions are summarized in Table I.

Table 1. Deformation analysis conditions

	Relaxation analysis	Loading analysis
Potential function	Tersoff	Tersoff
Ensemble	NPT	Volume change
Temperature	300 K	300 K
Time step	1.0 fs	1.0 fs
Total step	10^4	10^6
Deformation velocity	–	2.0 m/s

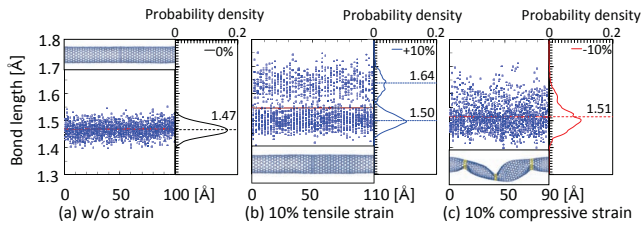


Figure 1. Estimated deformation and the distribution of C-C bond length of a (17, 0) CNT under uni-axial strain

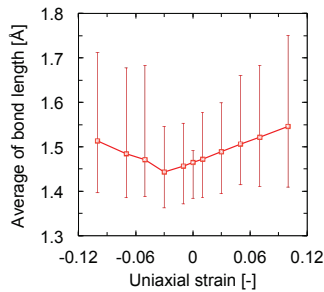


Figure 2. Change of the average of bond length of (17, 0) CNT under uni-axial strain

Figure 1 shows examples of the estimated distributions of C-C bond length of the CNT under an axial strain. A red line in each figure shows an average value of the bond length in the CNT. The bond length varied 1.41 to 1.55 Å in the CNT without strain and its average bond length was 1.46 Å. This value agreed with the experimental value [14]. The average distance increased monotonically with the increase of the applied strain as shown in Fig. 2. Figure 1(b) shows that the bond length distribution was separated into two major parts when the value of tensile strain was 10%. One was in the range of 1.50 ± 0.4 Å and the other was 1.64 ± 0.8 Å. The ratio of these average bond length was about 1.1 in this case. The zigzag CNTs also have two separated distributions of C-C bonds in terms of the bond direction, (A) C-C bonds not parallel to the tube axis and (B) those parallel to the axis. Therefore, the estimated separation of the bond length distribution indicates that bond lengths of type B (parallel to the tube axis) extended larger than bond lengths of type A (not parallel to the axis) and consequently six-membered rings in a CNT were distorted anisotropically under uniaxial tensile strain.

In the case of the axial compressive strain, the CNT showed simple shrinkage deformation when the amplitude of the applied compressive strain was less than 3% and then,

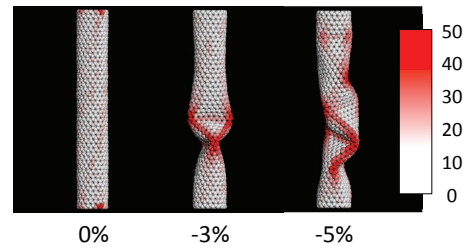


Figure 3. Change in the distribution of dihedral angle in (17, 0) CNT under 0, 3 and 5% compressive strain

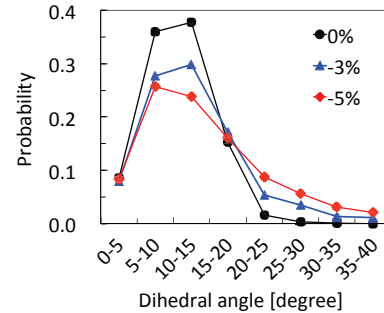


Figure 4. Change in the probability of the dihedral angle in (17, 0) CNT under 0, 3, and 5% Compressive strain

the average bond length decreased monotonically in this compressive strain region. The average bond length, however, increased when the amplitude of the applied compressive strain exceeded 3% (after buckling as shown in Fig. 1(c)). Figure 1(c) shows that the behavior of bond length change around buckling areas and that of other areas are different drastically with each other. Around the buckled areas, the range of the distribution of C-C bond length was much larger than that obtained from other areas.

Here we used a dihedral angle in order to visualize the area where deformation-induced orbital hybridization tend to occur. The dihedral angle is the angle between π orbitals of adjacent atoms. Figure 3 shows the change in the distribution of the dihedral angle in (17, 0) CNT as the increase in the compressive strain. The dihedral angle scale ranges from 0° to 50° , from white to red. In addition, the probabilities of the dihedral angle of these CNTs are shown in Fig. 4. While most dihedral angles are less than 20° at the relaxation state (0% strain), the dihedral angle distribution clearly shifted to a large dihedral angle, more than 20° . As mentioned at the following section, this dihedral angle value is around the critical value at which orbital hybridization occur in CNTs or GNRs. Thus, the buckling deformation of CNTs causes a very complicated conductivity change in the tube. This result indicates that the conductivity of CNT- based strain sensors should change drastically and complicatedly. Therefore, the clarification of the change mechanism of the electronic state of CNTs is a critical issue to develop a CNT-based strain sensor or electronic devices.

III. CHANGE OF ELECTRONIC STATE OF CNTs AND GNRs UNDER STRAIN

As was studied by previous studies, the electronic state of CNTs change significantly under axial, torsional [9], [10] and radial [15], [16] strain. Under axial and torsional strain, bond length change mainly causes the electronic state change and the band gap change can be solved analytically when a strain is small [9], [10]. It has also been revealed that radial strain causes orbital hybridization in a CNT which change the band gap. Although previous studies have focused on homogenous strain field, deformation of CNTs is more complicated as mentioned in the previous section. Thus, it is a critical issue to understand the effect of inhomogeneous strain on the electronic state of CNTs. In this section, focusing on orbital hybridization, we analyzed the electronic state of CNTs and graphene nanoribbons (GNRs) under three-dimensional strain field and compared there analysis results in order to understand how orbital hybridization is induced under deformation.

The change of the electronic band structure of the deformed GNRs and CNTs were analyzed by using Accelrys' DFT-code DMol³ [17], [18], and the DFT based on the generalized gradient approximation (GGA) of PW91 [19]. The total energy was converged to within 0.5 meV with a Monkhorst-Pack k-point mesh of $1 \times 1 \times 50$. Vacuum separations along both a and b axes were more than 50 Å, which was large enough to neglect the interaction of next cells. The length along c axis was equal to the transverse vector of GNRs and CNTs. We modeled armchair GNR (AGNR) ($N = 10, 16, 18, 20$) folded on a center line as shown in the inset of Fig. 5, where N is the number of atomic lines of AGNR. Each model consists of $2N$ carbon atoms and four terminated hydrogen atoms and their transverse length is 4.26 Å. $(n, 0)$ CNTs ($n = 9, 11, 12, 13$) under axial and radial strain were also modeled as shown in the inset of Fig. 6. Under the axial strain, transverse length of the CNT is $T = (1 + e) T_0$, where e is the axial strain and $T_0 = 4.26$ Å. The shape of cross sectional surface is fixed as an ellipse. The bond lengths of adjacent atoms are fixed during the radial strain loading in order to exclude the effect of the bond length change on the electronic state. The band gap change of GNRs and CNTs as the increase in maximum dihedral angle are shown in Figs. 5 and 6, respectively, where the dihedral angle is the angle between π orbitals of adjacent atoms.

In the case of large band gap GNRs and CNTs, the band gap started to decrease at a certain value of the dihedral angle, about 18° and 27° for GNRs and CNTs, respectively. In the case of small band gap GNRs and CNTs, the band gap did not change as much as large gap GNRs and CNTs. As for the decreasing rate of the band gap, that of CNTs were larger than that of GNRs. This should be because orbital hybridization were induced around areas of large dihedral angle which were larger in CNTs than in GNRs. A change of the band structure of AGNR ($N = 10$), a typical change of the band structure change, is shown in Fig. 7. The left, middle and right figures show the band structures of the pristine

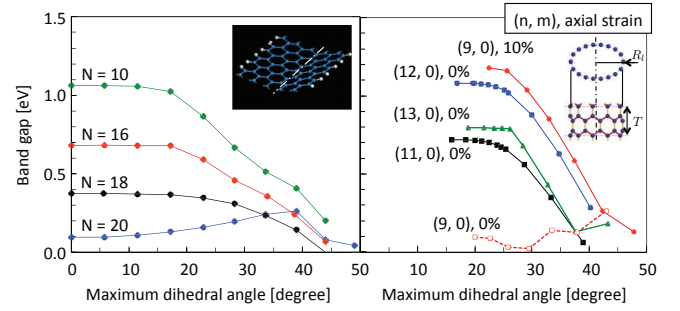


Figure 5. Change in the band gap of (a) folded GNRs and (b) CNTs under axial and radial strain as the increase in the maximum dihedral angle

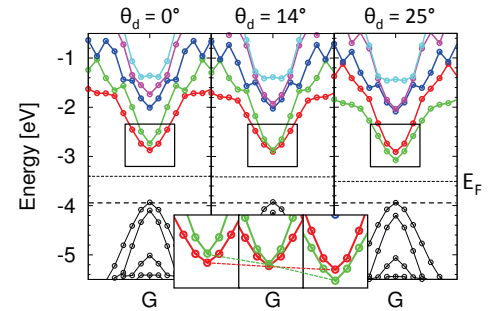


Figure 6. Change of the electronic band structure of folded AGNR ($N = 10$)

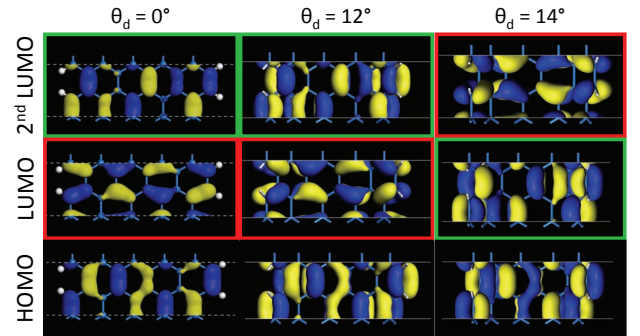


Figure 8. Spatial distributions of wave functions of deformed GNRs

GNR, the folded GNR of $\theta_d = 14^\circ$ and 18° , respectively, where θ_d is the maximum dihedral angle. This band structure change clearly shows that orbital hybridization caused the band gap change. When the dihedral angle was small ($\theta_d = 0-14^\circ$), the second lowest unoccupied molecular orbital (LUMO) energy decreased while the first LUMO and the highest occupied molecular orbital (HOMO) energy did not decrease significantly. After the second LUMO merged with the LUMO at the critical energy ($\theta_d = 14^\circ$), the LUMO energy started to decrease. The change of the first and second LUMO energies are shown in the inset of Fig. 7. Because both the LUMO and the HOMO energies did not change significantly, the band gap did not change significantly as shown in Fig. 1 when the dihedral angle was

small. Therefore, the band gap can be controlled by introducing the orbital hybridization. In addition, our study revealed that the generation of orbital hybridization can be predicted by analyzing the geometric structure of GNRs and CNTs. Thus, the estimation of the local electronic structure of GNRs or CNTs under buckling deformation can be possible by analyzing their geometric structure. This knowledge is very important to design the electronic devices or sensors based on carbon nanostructures.

To better understand the effect of the strain on the electronic states, we also analyzed spatial distributions of wave functions. Figure 8 shows the change of the HOMO, LUMO and the second LUMO of $N = 10$ AGNR under three different folded deformation at the G point. The states of these subbands can be classified into two groups: the vertical bonds along the axis direction (denoted as VB) and the parallel bonds perpendicular to the periodic direction (denoted as PB) [20]. While the maximum dihedral angle was small, the HOMO and the second LUMO were VB state and the LUMO was PB state. However, when the maximum dihedral angle exceeded the critical value ($\theta_d = 14^\circ$), the LUMO and the second LUMO states were tuned to be VB and PB states, respectively, although HOMO state did not change as the increase in the maximum dihedral angle. Clearly, the LUMO and the second LUMO were switched by the applied strain and this caused the band gap change as shown in Fig. 5.

IV. CONCLUSION

In this study, the change of the atomic configuration in CNTs and GNRs under deformation and its effect on their electronic band structures were analyzed by applying a MD and the DFT calculation. We found that the fluctuation of the atomic bond length and the dihedral angle between the adjacent carbon atoms are dominant structural parameters which change their electronic band structure. Because the increase in the dihedral angle should induce orbital hybridization in a deformed CNT, we analyzed the electronic state change of deformed CNTs and GNRs. Comparing analysis results of GNRs and CNTs, we found the relationship between the geometrical structure and the electronic state. Orbital hybridization induced at areas of orbital hybridization more than $10\text{-}20^\circ$ and $25\text{-}30^\circ$ in GNRs and CNTs, respectively. Such an anisotropic deformation occurs in a CNT under buckling deformation. The bond length and dihedral angle distribution in the buckled CNT changes drastically and complicatedly, and thus, its electronic band structure varies significantly. These analytical results clearly indicate the possibility of the development of a highly sensitive strain sensor using a CNT.

ACKNOWLEDGMENT

This research was partly supported by the Grants-in-Aid for Scientific Research and the Japanese special coordination funds for promoting science and technology.

REFERENCES

- [1] D. Qian, G. J. Wagner, W. K. Liu, M.-F. Yu, and R. S. Ruoff, "Mechanics of carbon nanotubes," *Appl. Mech. Rev.*, vol. 55, no. 6, p. 495, 2002.
- [2] J.-C. Charlier and S. Roche, "Electronic and transport properties of nanotubes," *Rev. Mod. Phys.*, vol. 79, no. 2, pp. 677–732, May 2007.
- [3] H. Shima, "Buckling of Carbon Nanotubes: A State of the Art Review," *Materials*, vol. 5, no. 12, pp. 47–84, Dec. 2012.
- [4] S. Iijima, C. Brabec, A. Maiti, and J. Bernholc, "Structural flexibility of carbon nanotubes," *J. Chem. Phys.*, vol. 104, no. 5, p. 2089, 1996.
- [5] R. Superfine, M. R. Falvo, G. J. Clary, R. M. Taylor, V. Chi, F. P. Brooks, and S. Washburn, "Bending and buckling of carbon nanotubes under large strain," *Nature*, vol. 389, no. 6651, pp. 582–584, Oct. 1997.
- [6] M. A. Cullinan and M. L. Culpepper, "Carbon nanotubes as piezoresistive microelectromechanical sensors: Theory and experiment," *phys. Rev. B*, vol. 82, no. 11, Sep. 2010.
- [7] E. Minot, Y. Yaish, V. Sazonova, J.-Y. Park, M. Brink, and P. McEuen, "Tuning Carbon Nanotube Band Gaps with Strain," *physical review letters*, vol. 90, no. 15, Apr. 2003.
- [8] R. J. Grow, Q. Wang, J. Cao, D. Wang, and H. Dai, "Piezoresistance of carbon nanotubes on deformable thin-film membranes," *Applied Physics Letters*, vol. 86, no. 9, p. 093104, 2005.
- [9] L. Yang, M. Anantram, J. Han, and J. Lu, "Band-gap change of carbon nanotubes: Effect of small uniaxial and torsional strain," *phys. Rev. B*, vol. 60, no. 19, pp. 13874–13878, Nov. 1999.
- [10] L. Yang and J. Han, "Electronic Structure of Deformed Carbon Nanotubes," *physical review letters*, vol. 85, no. 1, pp. 154–157, Jul. 2000.
- [11] T. W. Tomblor, C. Zhou, L. Alexseyev, J. Kong, H. Dai, L. Liu, C. S. Jayanthi, M. Tang, and S.-Y. Wu, "Reversible electromechanical characteristics of carbon nanotubes under local-probe manipulation," *Nature*, vol. 405, no. 6788, pp. 769–772, Jun. 2000.
- [12] C. Stampfer, A. Jungen, R. Linderman, D. Oberfell, S. Roth, and C. Hierold, "Nano-Electromechanical Displacement Sensing Based on Single-Walled Carbon Nanotubes," *Nano letters*, vol. 6, no. 7, pp. 1449–1453, Jul. 2006.
- [13] S. Plimpton, "Fast Parallel Algorithms for Short-Range Molecular Dynamics," *Journal of Computational Physics*, vol. 117, no. 1, pp. 1–19, Mar. 1995.
- [14] C. M. Lieber, T. W. Odom, J.-L. Huang, and P. Kim, "Atomic structure and electronic properties of single-walled carbon nanotubes : Article : Nature," *Nature*, vol. 391, no. 6662, pp. 62–64, Jan. 1998.
- [15] C.-J. Park, Y.-H. Kim, and K. J. Chang, "Band-gap modification by radial deformation in carbon nanotubes," *phys. Rev. B*, vol. 60, pp. 10656–10659, Oct. 1999.
- [16] J. Q. Lu, J. Wu, W. Duan, F. Liu, B. F. Zhu, and B. L. Gu, "Metal-to-semiconductor transition in squashed armchair carbon nanotubes," *physical review letters*, vol. 90, no. 15, p. 156601, 2003.
- [17] B. Delley, "An all-electron numerical method for solving the local density functional for polyatomic molecules," *J. Chem. Phys.*, vol. 92, no. 1, pp. 508–517, 1990.
- [18] B. Delley, "Fast Calculation of Electrostatics in Crystals and Large Molecules," *J. Phys. Chem.*, vol. 100, no. 15, pp. 6107–6110, Jan. 1996.
- [19] J. P. Perdew, K. A. Jackson, M. R. Pederson, D. J. Singh, and C. Fiolhais, "Atoms, molecules, solids, and surfaces: Applications of the generalized gradient approximation for exchange and correlation," *phys. Rev. B*, vol. 46, no. 11, pp. 6671–6687, Sep. 1992.
- [20] L. Sun, Q. Li, H. Ren, H. Su, Q. W. Shi, and J. Yang, "Strain effect on electronic structures of graphene nanoribbons: A first-principles study," *J. Chem. Phys.*, vol. 129, no. 7, p. 074704, 2008.